ANNALI DI GEOFISICA, VOL. XXXVII, N. 5, September 1994

Determination of Moho depth and dip beneath MEDNET station AQU by analysis of broadband receiver functions

Antonella Megna and Andrea Morelli
Istituto Nazionale di Geofisica, Roma, Italy

Abstract
We applied the receiver function technique to retrieve Moho depth and dip beneath the MEDNET very-broadband seismographic station at l'Aquila, in the Central Apennines. Broadband data available for teleseismic events recorded in two years of operation were sufficient to delineate a rather simple structure consisting of a 32-34 km thick crust, in agreement with previous studies based on refraction seismics. In addition, the data show relatively large variation in the amplitude of the converted *P*-to-*S* phase generated at the crust-mantle interface as a function of azimuth. These variations are consistent with synthetic receiver functions generated for an incident *P* wave interacting with an interface dipping ~ 8° to the north. Observations of amplitude ratios of converted phases, polarity of first-motion in the SH direction, and relative travel time delay are all consistent with a model assuming a Moho discontinuity about 33 km deep gently dipping towards north. The receiver function technique has shown to be an efficient tool for investigating deep crustal structure, giving localized but reliable information.

Key words *receiver function – Moho – converted phases – Central Apennines*

1. Introduction

Characterisation of the detailed structure of the crust and upper mantle is an important goal for geophysical studies. A reliable image of the crust-mantle transition is of fundamental importance to understand the tectonic environment and the geodynamic evolution of an active region such as the Italian Apennine mountain belt. Technical limitations of the different approaches are usually the source of uncertainty in our knowledge of subsurface structure. In fact, a really complete and reliable model must be based on the interpretation of several, different, geophysical observables. In the range of possible techniques, teleseismic *P*-wave receiver function modelling is of particular interest, because on the basis of data recorded by a single three-component broadband seismograph it is able to yield precise, though geographycally pointlike, information on deep crustal and upper mantle structure.

The receiver function technique is based on the identification and modelling of phases converted and reverberated at the free surface and at the Moho interface. This allows to reconstruct depth and possible dip of reflecting and refracting interfaces. The technique, first suggested by Langston (1979) and more recently examined in detail by Owens *et al.* (1984) is based on teleseismic *P* waveform processing to isolate the *P*-to-*S* converted phases (receiver functions) on the horizontal components. These converted phases are the result of the *P* wave interaction with the discontinuity surfaces in the crust.

The presence of dipping interfaces changes the amplitude of the *P*-to-*S* converted phase with respect to azimuth around the observation

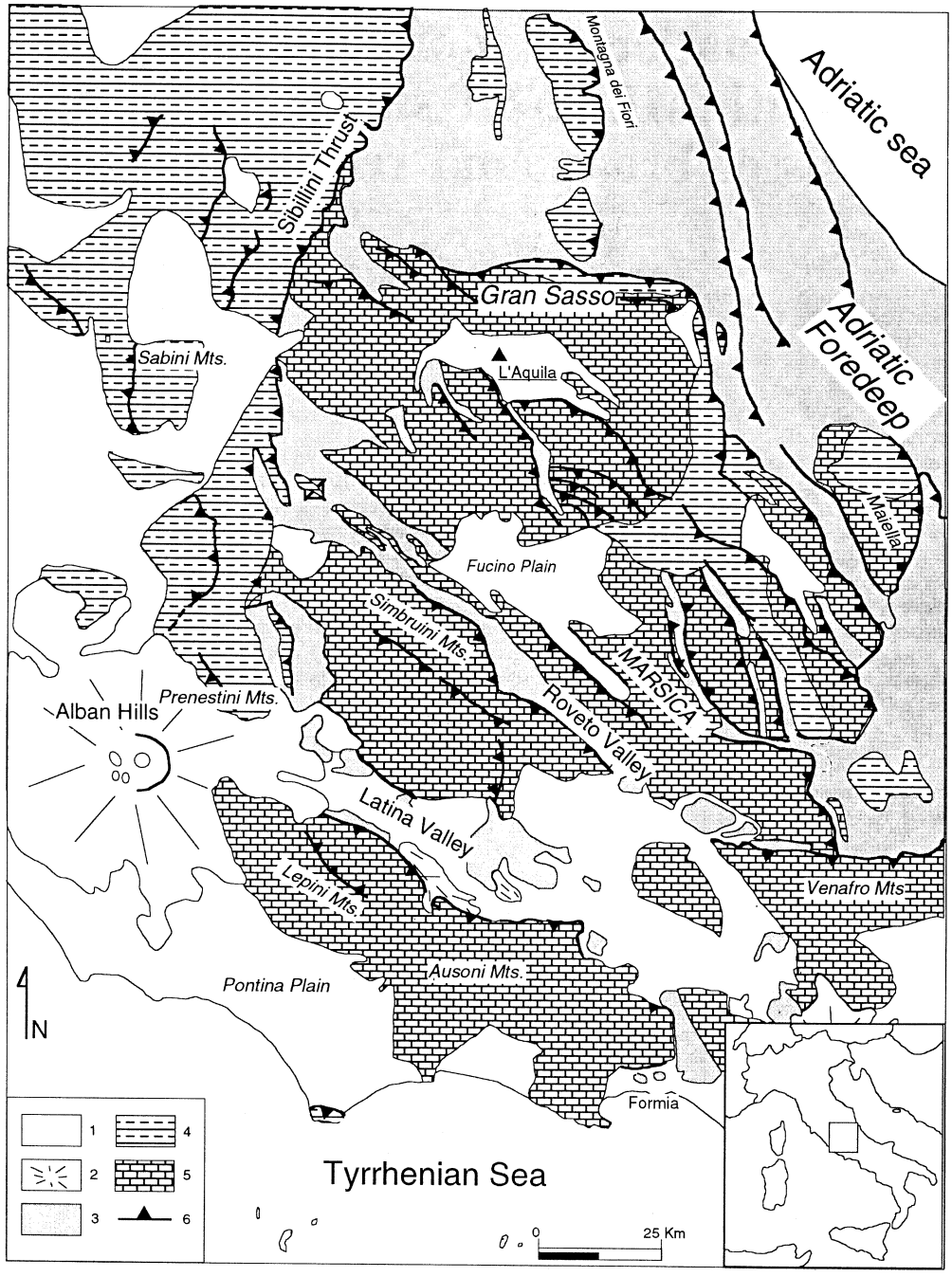

Fig. 1. Geologic map of the Central Apennines (courtesy of M. Mattei). 1) sediments of Pliocene-Quaternary; 2) volcanic cover; 3) sediments of Miocene; 4) Umbria-Marche domain; 5) Latium-Abruzzi carbonate platform; 6) main thrust fronts.

point, and generates a direct arrival also on the tangential (SH) component.

In this paper we show an application of the technique to teleseismic *P* waveforms recorded at a single very-broadband seismographic station of the MEDNET network, located at l'Aquila in the Italian Central Apennines (fig. 1). An important advantage of this technique is that it can contribute to a better delineation of the structure of the crust with only one station (Langston, 1979; Owens *et al.*, 1984; Owens, 1987). Lateral variations of the structure around the station may be obtained with a good approximation by examining the azimuthal variation of one-dimensional vertical velocity distributions.

In literature one can find many information from seismic refraction profiles on the crustal structure of the Northern and Southern Apennines (Mostardini and Merlini, 1986; Nicolich, 1981). On the contrary, the knowledge of such a structure in the Central Apennines is poor of data (Cassinis, 1983; Geiss, 1987; Giese and Morelli, 1975), but from these few information one can infer that the Moho depth in the region of Central Italy is about 30-35 km.

2. Geological setting

In the Mediterranean region the collision between the Eurasian and the African continental plates caused a complex tectonic evolution with the formation of subsystems of different tectonic regimes (compressional, extensional and transcurrent). Several thrust belts were formed by this complex tectonics, as for example the Apennines.

The formation of the Apennine thrust belt in the Italian region started in the lower Miocene. After an intense phase of compressional tectonics, an extensional regime initiated in the Upper Miocene, with the formation of the Tyrrhenian Sea. During this phase – still continuing, as shown by the presence of intense seismic activity in the crust and the upper mantle (Selvaggi and Amato, 1992) – the Latium-Abruzzi carbonatic platform and the basinal units of the Umbria-Marche-Sabina domain have moved towards the Adriatic foredeep (Salvini and Tozzi, 1986), being fragmented into several blocks. This NE migration caused the formation of tectonic structures with Apenninic NW-SE direction.

The seismic station of l'Aquila is located about 10 km to the south of the Gran Sasso massif, which is in the northern sector of the Latium-Abruzzi carbonatic platform (Castellarin *et al.*, 1978). Cross sections of this area show the overthrust of the carbonate platform onto buried basin domain of Umbria-Marche with a northern vergency (Parotto and Praturlon, 1975; Ghisetti and Vezzani, 1986).

3. Broadband receiver function analysis

For this study we have analysed teleseismic events recorded by the MEDNET station AQU. MEDNET is the very-broadband seismographic network installed around the Mediterranean by the Istituto Nazionale di Geofisica and supported by the World Laboratory. The project currently consists of 15 stations – installed in 10 Countries – in cooperation with local seismological institutions and other international projects (the French program GEOSCOPE, the American consortium IRIS). Hardware is based on STS1/VBB sensors and Quantagrator 24-bit A/P converters. This station configuration provides flat velocity response in the frequency band between 3 mHz and 8 Hz (fig. 2), with a full dynamic range larger than 140 dB. More details on the MEDNET network may be found in Boschi *et al.* (1991).

To know the response of the crust and upper mantle structure, termed receiver function, the teleseismic *P* wavetrain must be analysed so as to identify the contribution to the complexity of the waveform given by the structure near the receiver. Source and long-range propagation effects must therefore be removed. To determine the presence of interfaces with high velocity contrast in the crust we are primarily interested in converted phases of the *P*-to-*S* type. The horizontal components of the receiver function are then isolated using an empirical deconvolution procedure (Langston, 1979). This approach is based on the representation of the teleseismic *P* signal recorded at a

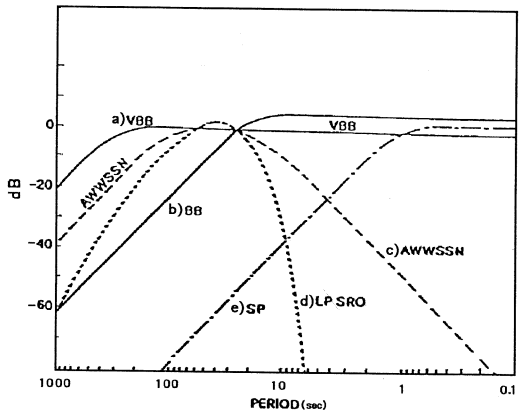

Fig. 2. Frequency response of the VBB instrument (a) compared to other standard seismographs: broadband (b), WWSSN (c), long-period SRO (d), short-period SRO (e). The horizontal scale spans frequencies between 1 mHz and 10 Hz.

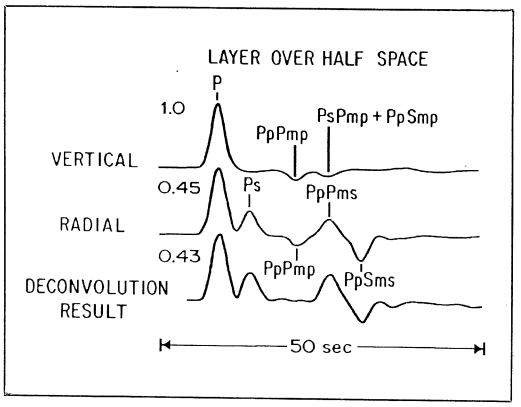

Fig. 3. Test of deconvolution technique with synthetic data computed for a layer over a half space. The two top traces show the synthetic response on vertical and horizontal radial components. The bottom trace is the result of the deconvolution procedure on the radial component. The number above any trace is the *P* amplitude ratio with respect to the *P* wave of vertical component (after Langston, 1979).

station as the convolution of a source function, path effects, near-receiver structure response, and an instrumental transfer function. For teleseismic events the waveform is relatively simple since propagation effects produced by the mantle structure are small. Theoretical calculations for typical crustal structures show that reverberations and converted phases amplitude on the vertical component are very small since the angle of incidence is very close to vertical (Burdick and Langston, 1977; Langston, 1977). This is shown in the top trace of fig. 3. The vertical component then primarily contains the effects of source, long-range propagation, and instrument response. The source function, mantle propagation and the instrumental response are therefore removed by deconvolving the vertical component from the horizontal radial and tangential components. The receiver function allows an easy identification of converted waves of the *P*-to-*S* type caused by *P* wave interaction with discontinuities. Finally, the deconvolved seismograms are convolved with a simple gaussian time function to exclude high frequency signal.

For this study we have selected 30 events with epicentral distance between 25° and 90°, and magnitude around 6.0 or greater (table I). With these epicentral distances the seismic rays cross the crust and upper mantle with a very steep incidence angle. We have selected only events with magnitude larger than 6.0 to have a better signal-to-noise ratio.

These events are grouped into five distinct sets with respect to their back azimuth (fig. 4). Each group is a cluster of events with similar estimates of their receiver functions. The subdivision of these groups was done empirically, considering both event back azimuth and similarity of receiver functions, to avoid grouping together waveforms with incompatible characters. Horizontal radial receiver functions for events of group B, the most numerous, are shown as an example in fig. 5. Similarity of the main characters of these functions allowed to stack them, in the time domain, to derive a single, average, receiver function for each group. Groups A and B are rather similar (see fig. 6a,b) but we preferred to divide them because of a difference in arrival times of rever-

Table I. Teleseismic events recorded at the station of L'Aquila and analysed in this study.

Event	Date	Lat. (N) (deg)	Long. (E) (deg)	Dist. (deg)	Baz (deg)	M_b
1	12 03 90	51.484	– 175.032	86.25	5.275	6.0
2	25 03 90	9.919	– 84.808	89.39	282.788	6.2
3	26 04 90	35.986	100.245	64.80	63.507	6.5
4	01 05 90	58.840	– 156.858	78.84	354.857	6.1
5	08 05 90	6.905	– 82.622	89.83	279.120	6.2
6	12 05 90	49.037	141.847	78.34	31.756	6.5
7	17 05 90	26.619	127.846	88.59	54.610	6.0
8	20 05 90	5.121	32.145	40.65	150.578	6.7
9	14 06 90	47.869	85.076	49.21	57.580	6.1
10	20 06 90	36.636	49.799	28.51	89.302	6.0
11	14 07 90	0.003	– 17.376	50.44	221.589	6.2
12	16 10 90	49.043	155.076	82.94	24.280	6.0
13	25 10 90	35.121	70.486	44.38	79.665	6.0
14	06 11 90	28.251	55.462	36.72	98.720	6.2
15	06 11 90	53.452	169.871	82.44	13.940	6.3
16	31 01 91	35.993	70.423	43.95	78.583	6.4
17	21 02 91	58.427	– 175.450	79.31	4.728	6.2
18	08 03 91	60.904	167.023	74.87	13.002	6.4
19	04 04 91	7.017	– 78.153	86.48	276.215	6.1
20	22 04 91	9.685	– 83.073	88.30	281.457	6.3
21	01 05 91	62.476	– 151.413	74.81	352.757	6.1
22	30 05 91	54.567	– 161.606	83.61	357.077	6.3
23	10 06 91	23.771	– 45.368	51.60	268.413	6.1
24	06 08 91	3.827	95.374	81.50	92.574	6.0
25	17 08 91	40.235	– 124.348	89.32	329.020	6.0
26	17 08 91	41.821	– 125.397	88.34	330.493	6.2
27	26 11 91	42.051	142.523	84.28	35.502	6.1
28	13 12 91	45.578	151.560	84.84	28.064	6.1
29	13 12 91	45.521	151.707	84.94	28.002	6.1
30	19 12 91	45.253	151.176	84.98	28.462	6.0

berations after the *Ps* peak. Average horizontal radial receiver functions for the groups modelled are shown in figs. 6a-d, along with bounds constructed around the stack plus and minus the standard deviation. This is done to give a qualitative idea of variation within each group. The dashed traces, also shown in figs. 6a-d, superimposed on average traces, represent synthetic receiver functions computed applying the same deconvolution procedure to synthetic seismograms calculated with a reflectivity algorithm (Kennett, 1983) in models described as follows.

Transverse receiver functions are subject to relatively large instability in the presence of noise (Langston, 1981), as well as sensitive to

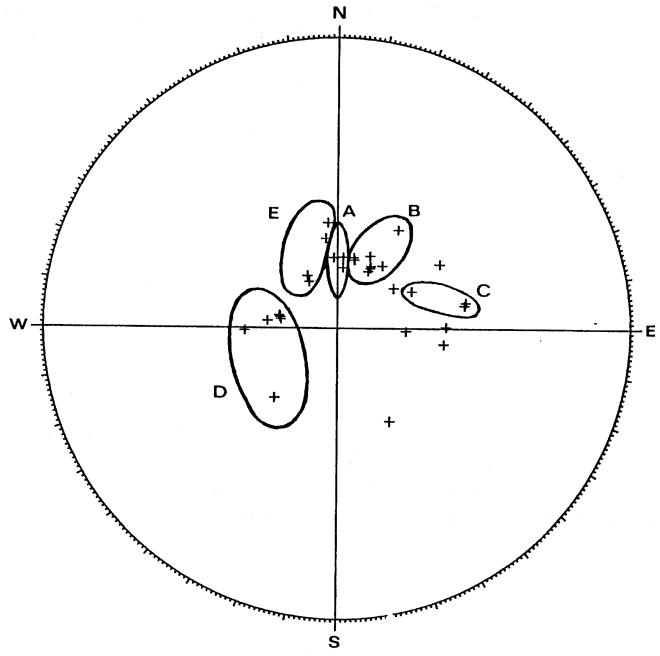

Fig. 4. Distribution of the events of table I. Lower hemisphere, Schmidt projection of incidence angle azimuth at station AQU.

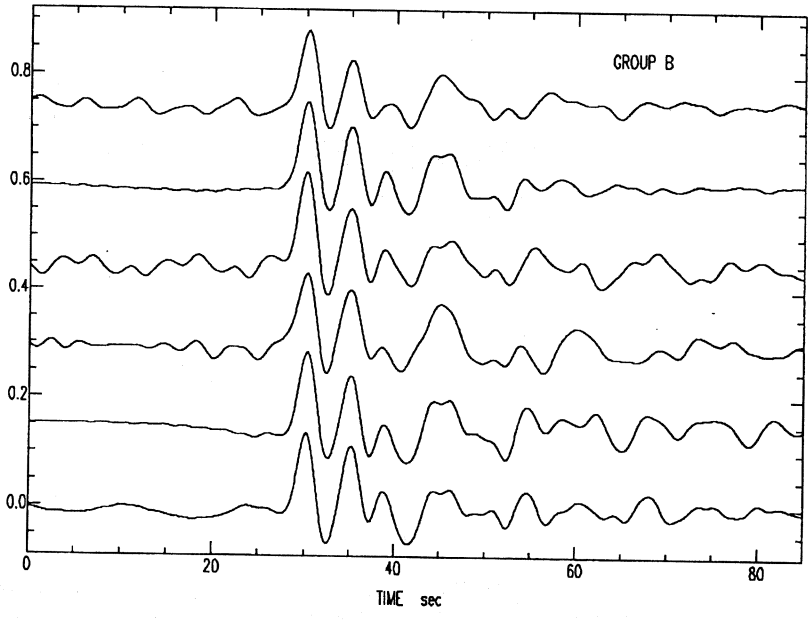

Fig. 5. Radial receiver functions of the events of group B.

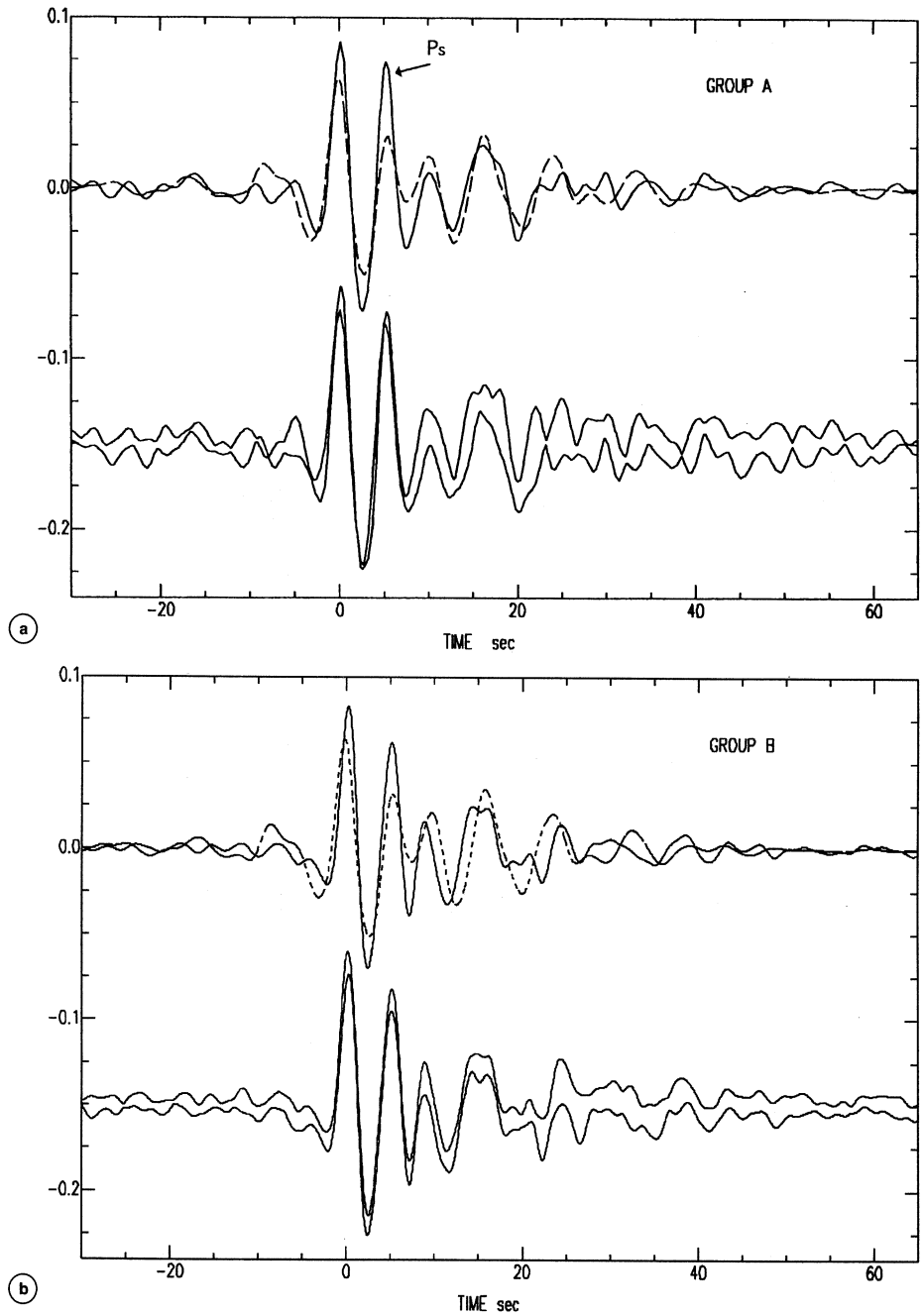

Fig. 6a,b. Stacked radial receiver functions of groups A and B. Top: the solid trace in each frame is the average receiver function; bottom: the two traces are the bounding receiver functions representing $\pm 1\sigma$ about the average. The dashed traces are synthetic receiver functions computed by assuming as average values for crustal and upper mantle velocities those of table II.

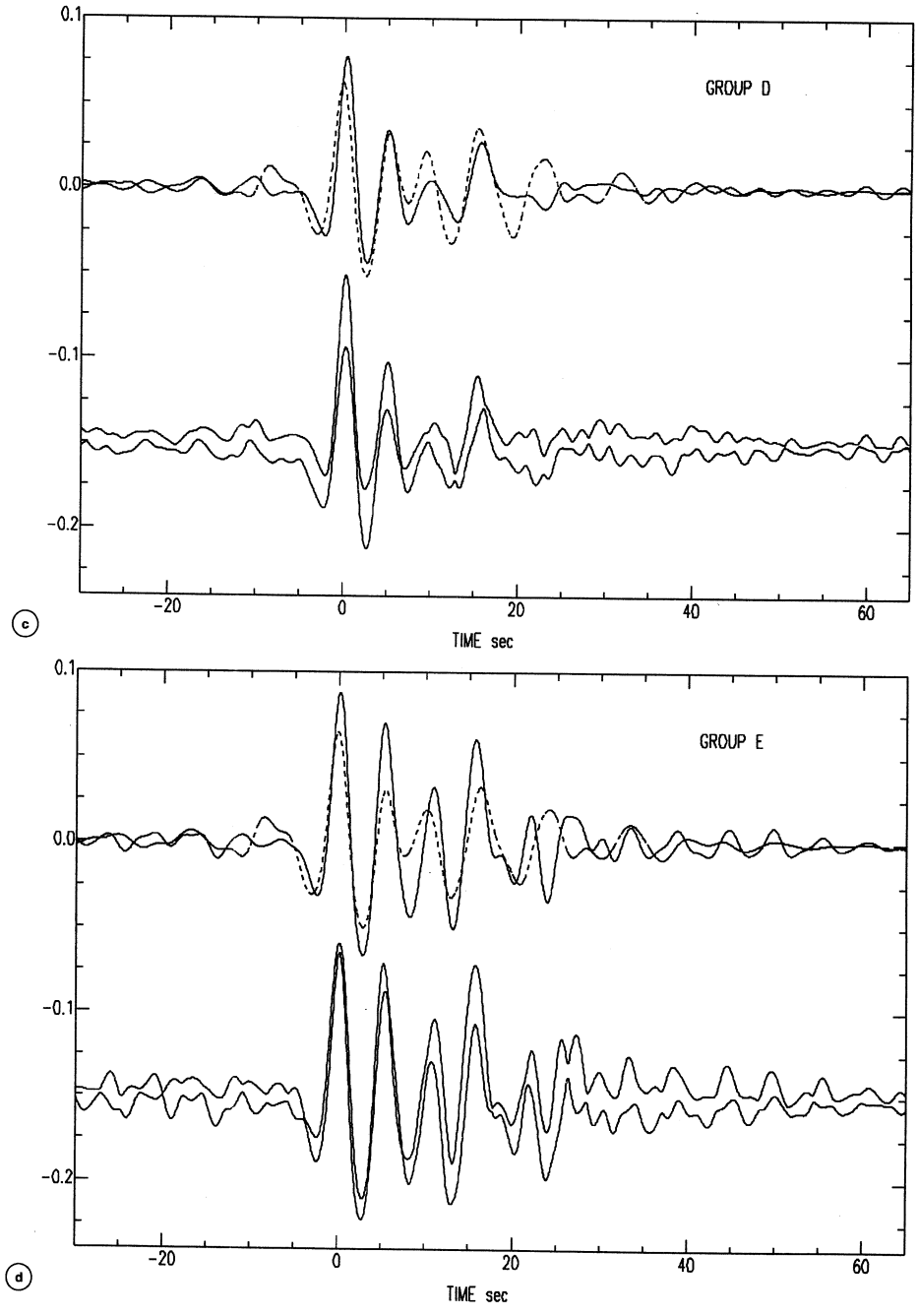

Fig. 6c,d. Stacked radial receiver functions of groups D and E. Top: the solid trace in each frame is the average receiver function; bottom: the two traces are the bounding receiver functions representing $\pm 1\sigma$ about the average. The dashed traces are synthetic receiver functions computed by assuming as average values for crustal and upper mantle velocities those of table II.

effects of shallow structure. Therefore in this study the analysis of receiver functions is limited to a detailed analysis of the (horizontal) radial data, whereas transverse data will only be used for polarization analysis of the first pulse.

The most apparent characters of the functions in figs. 6a-d are the amplitude and the time delay of the main peak after the direct *P* arrival (at time 0), corresponding to *Ps* conversion. Moho depth, *S*-wave velocity in the crust, and velocity contrast at the Moho influence time and amplitude of this peak. In this article we will always consider a homogeneous crust as we are, at this stage, interested in deriving gross characters of the crust on the basis of forward modelling. Crustal reverberations, including *P* legs in the Moho and arriving later in the seismogram, are also sensitive to υ_P in the crust.

4. Discussion

The stacked receiver functions, obtained by the technique described above for the five groups, contain detailed information about the crustal structure beneath the seismographic station. A first approximation to estimate crustal thickness and interface velocity contrast can be obtained by modelling arrival time and amplitude of converted *Ps* waves in the time domain.

To better understand the receiver functions we calculated synthetic seismograms based on one-dimensional, layered, Earth structure. Our starting model is a modification of global travel time model SP6 (Morelli and Dziewonski, 1993; fig. 7) where we merged the first two layers (upper and lower crust) into one homogeneous layer (homogeneous crust), and assumed as average values for crustal and upper mantle velocities those estimated by Cassinis (1983) for the Central Apennines (table II). In our modelling we allowed both crustal thickness and velocity to vary to fit the observed receiver function.

The synthetic seismograms computed for the starting model show a good estimate of receiver functions in terms of arrival times of the converted *Ps* phases (figs. 6a-d), but not in terms of amplitude. Indeed groups A, B and E exhibit an amplitude of converted *Ps* waves larger than that of synthetic seismograms. This does not occur for group D which is well fit (group C has not been studied because the waveform is not as simple as that of the previous groups, and its modelling was not possible within the assumptions made).

In our model we assumed a high velocity contrast at the Moho (2.3 km/s) to better fit the data, considering also available information on the Central Apennine structure (Cassinis, 1983). For a more common value of crustal velocity of 6.5 km/s the synthetic waveforms show very small *Ps* phase amplitude, and later arrival time of the first reverberation

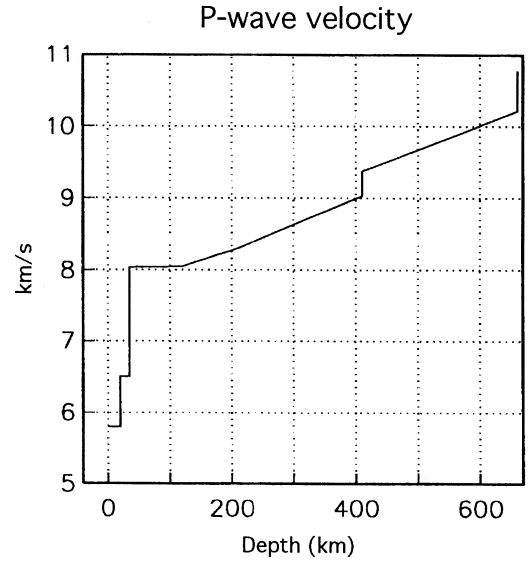

Fig. 7. Upper mantle *P* and *S* velocity in model SP6.

Table II. Average values of velocities for the crust and the upper mantle in the Central Apennines estimated by Cassinis (1983).

Layer	V_P (km/s)	V_S (km/s)	Density (kg/m^3)	Depth (km)
1	6.0	3.2	2.7	0.0
2	8.3	4.8	3.3	33.0

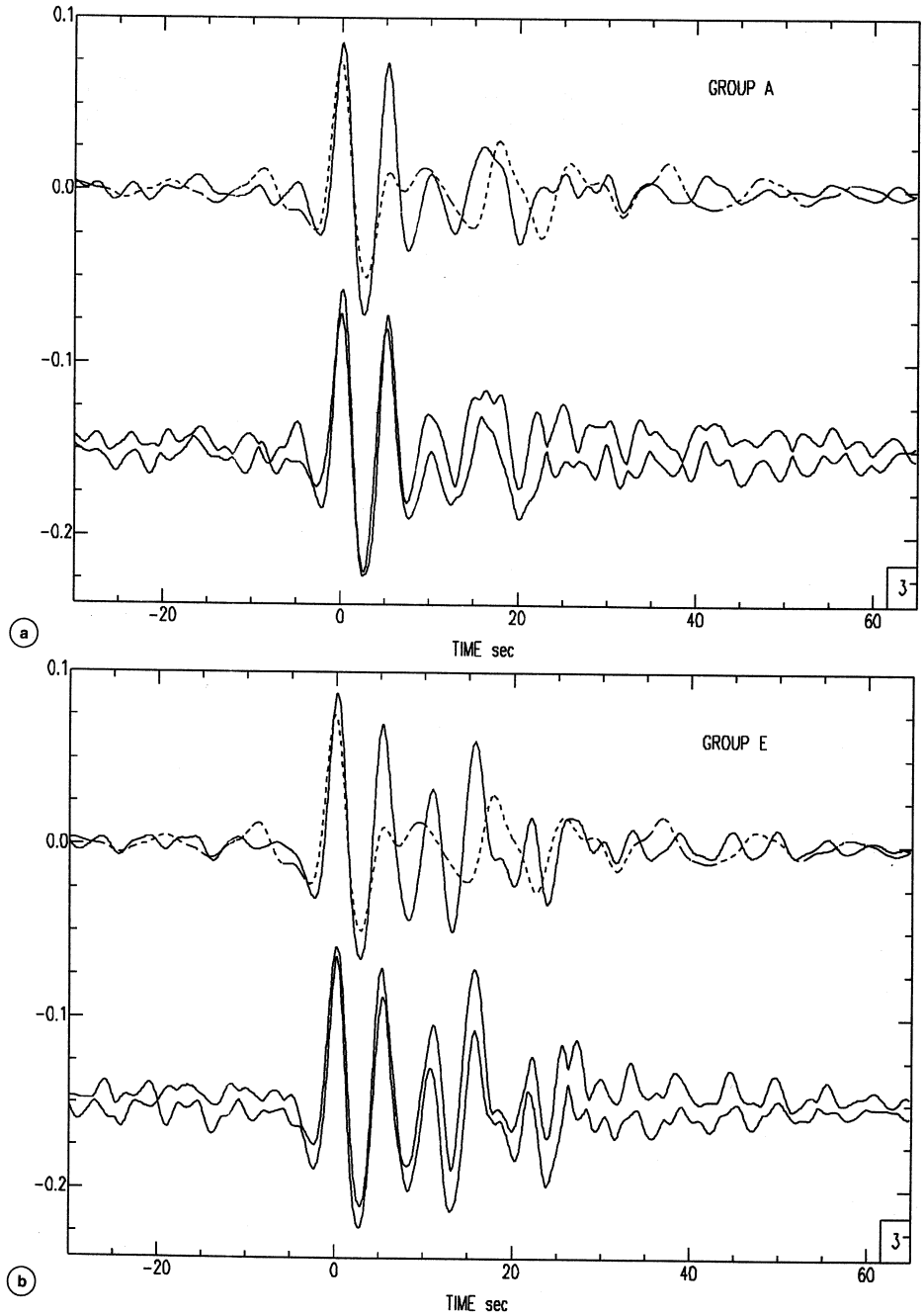

Fig. 8a,b. Stacked radial receiver functions of groups A and E. Top: the solid trace in each frame is the average receiver function; bottom: the two traces are the bounding receiver functions representing $\pm 1\sigma$ about the average. The dashed traces are synthetic receiver functions computed by assuming 6.5 km/s as average value of crustal velocity.

(fig. 8a,b). To model the arrival time of the *Ps* phase we must then use a Moho depth (43 km) larger than the known values for the Central Apennines (Cassinis, 1983; Geiss, 1987; Giese and Morelli, 1975). To obtain *Ps* phase amplitude as large as observed, we should instead assume a velocity contrast even larger than 2.3 km/s; but it is very unlikely.

An other character to consider for the modelling of crustal structure is the different amplitude of *Ps* phase with respect to back azimuth. In an Earth model consisting of horizontal, laterally homogeneous layers, the amplitude of the converted *Ps* phase does not vary with back azimuth and decreases only slightly as distance increases (fig. 9). This is because the incidence angle of teleseismic rays varies very little for epicentral distances between 25° and 90°. This is no more true in the case of dipping interfaces, since each ray, depending on its back-azimuth, has a different incidence angle on the discontinuity. The consequence is the variation of amplitude ratios for converted waves.

All synthetic traces in figs. 6a-d have been computed for a horizontally homogenous, layered structure, but we can work with amplitude ratios *Ps/P* by explicitly computing them from ray theory. To justify these amplitude variations, we consider a crustal and upper mantle model with a dipping Moho interface (Owens *et al.*, 1988). In this case, teleseismic *P* waves with identical ray parameters, but with different back azimuth, will generate converted phases with different amplitude due to differences in the angle of incidence on the dipping interface. To illustrate this geometric effect, we computed the variation of the *Ps/P* amplitude ratio with respect to epicentral distance for model of table II, with a dipping interface (5°, 8° and 10°; fig. 10a-c). The *Ps/P* ratio increases rapidly as distance increases for updip back azimuths and decreases slightly for downdip rays. These tests indicate that the

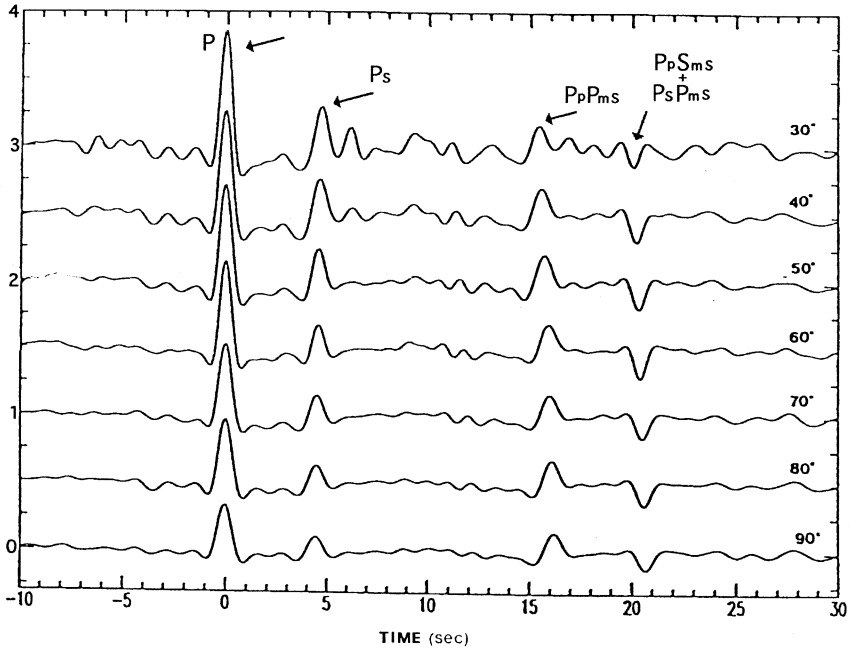

Fig. 9. Deconvolved radial component of synthetic waveforms computed for several epicentral distances.

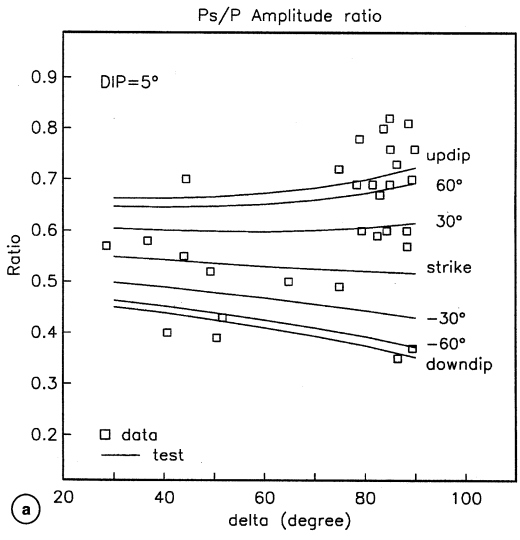

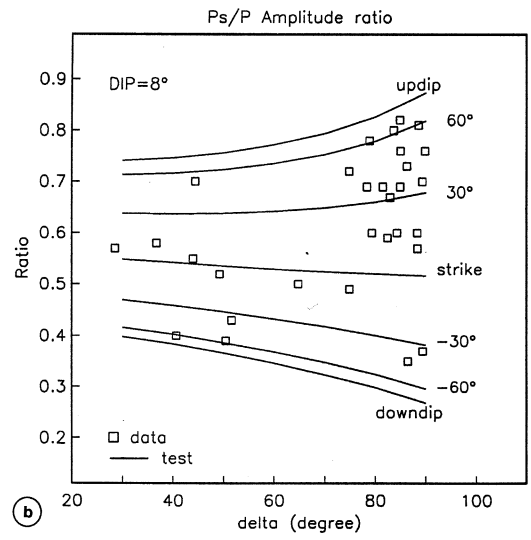

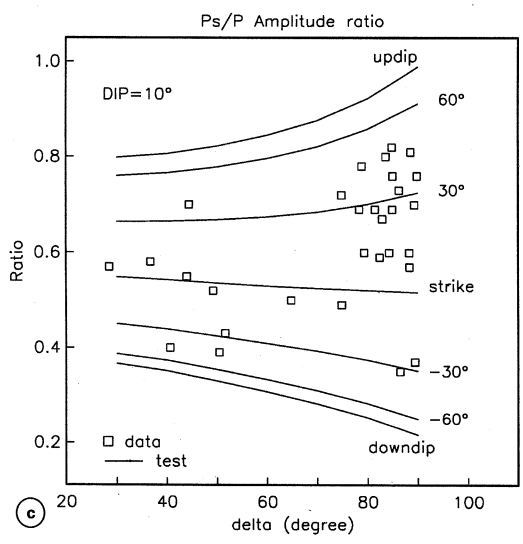

Fig. 10a-c. Variation in *Ps/P* amplitude ratio with respect to epicentral distance. The continuous lines describe the variation in *Ps/P* amplitude ratio computed for a model having a single dipping interface with a dip of 8° for several back-azimuths with respect to interface strike. Updip and downdip directions are the relative back-azimuths respectively of 90° and – 90°. The squares indicate the *Ps/P* amplitude ratios of data.

Ps/P amplitude ratio is sufficiently sensitive to surface dip to allow to model its geometry, and that the spread of values is consistent with a 8° dip.

Fig. 11 shows the variation of *Ps/P* amplitude ratio with respect to back azimuth. Most of the observations of *Ps/P* ratios with amplitude (0.57/0.82) larger than that calculated for the synthetic seismograms (0.52/0.55) are clustered at azimuth around N, whereas lower values are found for paths from the south (180°). Data are compared, in fig. 11, with lines showing theoretical variation as a function of azimuth for a dip of 8° toward north. Variation with epicentral distance (represented by lines in fig. 10a-c) is shown by the two curves com-

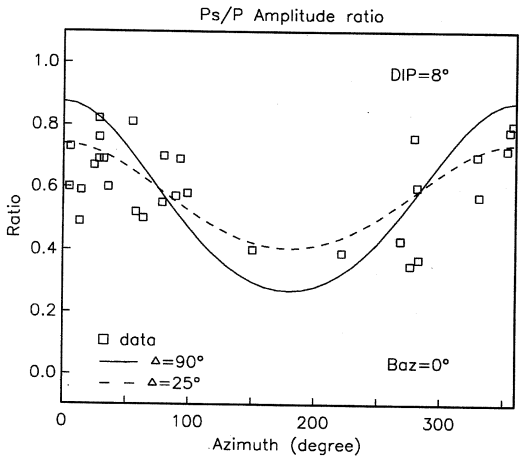

Fig. 11. Variation in *Ps/P* amplitude ratio with respect to back-azimuth. The continuous line and the dashed line describe the variation in *Ps/P* amplitude ratio computed for the epicentral distances respectively of 90° and 25° for a model having a single dipping interface towards north with a dip of 8°. The squares indicate the *Ps/P* amplitude ratio of data.

puted for 25° and 90° distance. From the analysis of fig. 11 we may conclude that data are consistent with a 8°, northward, dip of the Moho. Even if this interpretation is not unique, we will see that it is supported by other evidence.

If the Earth structure can be represented by a model consisting of horizontal, laterally homogeneous layers we will only see SH wave type on the tangential component. A dipping interface instead causes a non-zero contribution of the first arrival on the tangential component.

The presence of a dipping interface bends the ray path from the vertical toward the dip direction. In this way the tangential *P* wave components are azimuthally antisymmetric with respect to interface dip direction (Langston, 1977; Owens and Crosson, 1988). Plotting these polarities (fig. 12) we can infer that the dip direction is, again, generally toward north. This is also consistent with relative residuals of *Ps/P* times of each group (fig. 13),

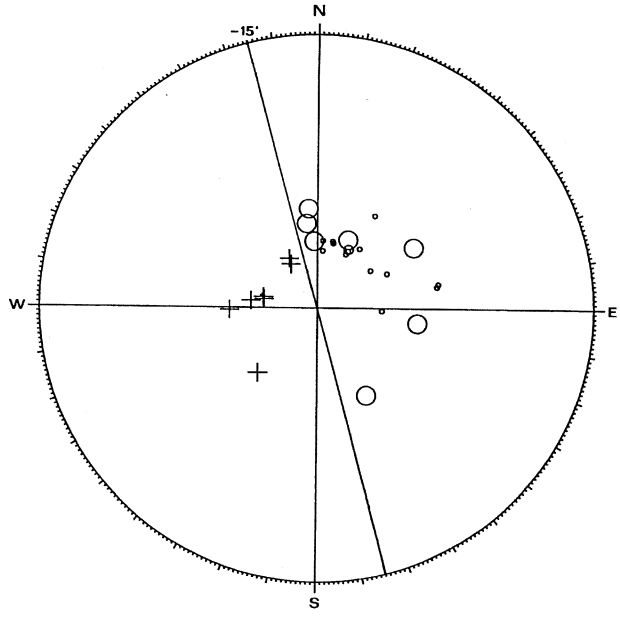

Fig. 12. Polarity of tangential *P* motion. The pluses indicate positive polarity, circles indicate negative polarity, and the small circles indicate events where no reliable determination could be made.

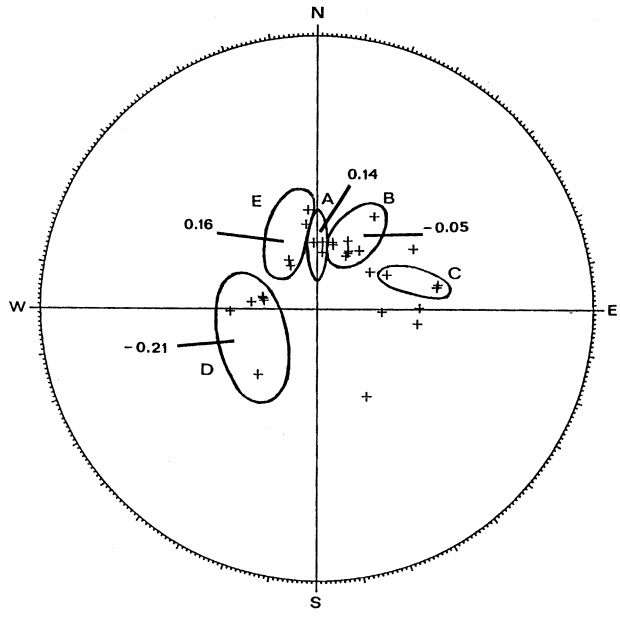

Fig. 13. Azimuthal distribution of residuals of *Ps/P* time. The residual *Ps/P* time of each group has been computed with respect to the average of time delays of all groups (5.0 s).

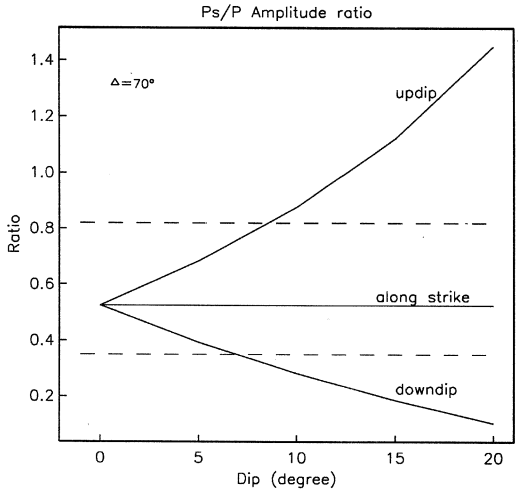

Fig. 14. Effect of interface dip on *Ps/P* amplitude ratio for a teleseismic distance of 70° (continuous line). The dashed lines indicate the maximum and minimum values of the experimental data.

even though travel times in the crust might be affected by lateral heterogeneities which we are not modelling.

The magnitude of the dip angle can also be estimated by computing the change in *Ps/P* amplitude ratio for updip and downdip directions for the same epicentral distance (fig. 14). The spread of experimental values, shown with a horizontal band in fig. 14, is such as to suggest a value of about 8° – as used previously – but, more reliably, included between 5° and 10°. The small value of the dip angle, and its northward direction, are consistent with the values of crustal thickness we determined by fitting average receiver functions. Indeed for the groups A and E the Moho depth is about 34 km, while it is respectively 33 and 32 km for the other two groups, B and D. An inclination of 8° would account for a difference of about 2-3 km in Moho depth where it is intersected by rays with updip and strike azimuths.

5. Conclusions

Analysis of broadband receiver functions is a rather reliable method to derive information on the structure of the crust and the Moho just below a seismograph station. Preliminary analysis of receiver functions computed for teleseisms recorded at MEDNET station AQU (l'Aquila) allowed to identify 5 groups on the basis of waveform similarity and back-azimuth. Similarity of receiver functions computed for paths with similar incidence and back-azimuth suggests that their characters are mainly controlled by near-receiver structure. Traces from each group can, subsequently, be stacked in order to increase signal-to-noise ratio and to limit the number of traces to model.

A first conclusion which may be drawn is, then, about the average crustal structure beneath station AQU. Comparison with synthetic receiver functions computed for a flat layered model reveals that a homogenous, 33 km thick crust is capable of reproducing the gross features found in the data. Such a model is consistent with previous determinations (Cassinis, 1983; Geiss, 1987; Giese and Morelli, 1975).

A closer look at the fit obtained by synthetic radial receiver functions for a flat layered structure reveals that there is a significant variation of the *Ps/P* amplitude ratio with varying azimuth. This can of course be explained with lateral variation of the structure. The simplest variation that we can model is represented by a dip of the Moho surface. Such a feature is mainly suggested by the coherent pattern of polarization of first *P* arrival, with energy on the horizontal transverse component not explained by a horizontal refraction surface. Polarity of first impulse on the transverse receiver function rather consistently changes sign along a line with an azimuth of about – 15°. This can be accomplished by a Moho dipping to NNW. More complicated features are also present on receiver functions suggesting a more complicated pattern for heterogeneity, possibly including variations of v_P and v_S. This is shown for instance by the difficulty to fit group C (eastward backazimuth) with a flat layered model. Such variations will need additional work and a larger set of data for the modelling.

Besides the average Moho depth of about 33 km, then, we can deduce that there is indication of a northern dip of the crust-mantle interface beneath AQU by 8°. These values may of course be affected by some uncertainty which we find, for the moment, difficult to quantify. They should, however, be considered as a first step toward a more precise determination of the crustal structure. We used a simple model, consisting of a homogenous crust. The receiver function technique by modelling both differential travel times and amplitude of converted and reverberated waves – can resolve between crustal thickness and wave velocity. However, we did not consider in the present study more complex models because we limited ourselves to a simple trial-and-error process for reproducing the observed waveforms. More resolution, as well as a better estimate of the uncertainty of the results, may be achieved by resorting to the formulation of a standard linearized inverse problem, currently under way.

Acknowledgements

We thank Alessandro Amato for useful suggestions and comments, and Enzo Boschi for continuing encouragement and discussion.

REFERENCES

BOSCHI, E., D. GIARDINI and A. MORELLI (1991): MEDNET: The very broadband seismic network for the Mediterranean, *Il Nuovo Cimento*, **14**, 79-99.

BURDICK, L.J. and C.A. LANGSTON (1977): Modelling crustal structure through the use of converted phases in teleseismic body-wave forms, *Bull. Seismol. Soc. Amer.*, **67**, 677-691.

CASSINIS, R. (1983): Seismicity and crustal structure in the Italian region: a preliminary zoning, *Boll. Geofis. Teor. Appl.*, **25**, 3-26.

CASTELLARIN, A., R. COLACICCHI and A. PRATURLON (1978): Fasi distensive, trascorrenze e sovrascorrimenti lungo la «Linea Ancona-Anzio», dal Lias medio al Pliocene, *Geol. Romana*, **17**, 161-189.

GEISS, E. (1987): A new compilation of crustal thickness data for the Mediterranean area, *Annales Geophysicae*, **5B**, 623-630.

GHISETTI, F. and L., VEZZANI (1986): Analysis of the Gran

Sasso-Morrone arc (Central Apennines, Italy), in *Atti 73° Congresso Soc. Geol. It.*, 133-136.

GIESE, P. and C. MORELLI (1975): Crustal structure in Italy, «Structural Model of Italy», CNR, *Quad. Ric. Sci.*, **90**, 453-489.

KENNETT, B.L.N. (1983): *Seismic wave propagation in stratified media* (Press Syndicate of the University of Cambridge).

LANGSTON, C.A. (1977): Corvallis, Oregon, crustal and upper mantle receiver structure from teleseismic *P* and *S* waves, *Bull. Seismol. Soc. Amer.*, **67**, 713-724.

LANGSTON, C.A. (1979): Structure under Mount Rainier, Washington, inferred from teleseismic body waves, *J. Geophys. Res.*, **84**, 4749-4762.

LANGSTON, C.A. (1981): Evidence for the subducting lithosphere under Vancouver Island and Western Oregon from teleseismic *P* wave convesions, *J. Geophys. Res.*, **86**, 3857-3866.

MORELLI, A. and A.M. DZIEWONSKI (1993): Body wave traveltimes and a spherically symmetric *P*- and *S*-wave velocity model, *Geophys. J.*, **112:2**, 178-194.

MOSTARDINI, F. and S. MERLINI (1986): *Appennino Centrale-Meridionale: sezioni Geologiche e Proposta di Modello Strutturale* (Agip, Roma), pp. 59.

NICOLICH, R. (1981): Il profilo Latina-Pescara e le registrazioni mediante OBS nel Mar Tirreno, in *Atti 1° Convegno GNGTS*, E.S.A., 621-633.

OWENS, T.J. (1984): *Determination of Crustal and Upper Mantle Structure from Analysis of Broadband Teleseismic P-waveforms*, Ph.D. Dissertation, University of Utah, Salt Lake City, Utah, 146.

OWENS, T.J., (1987): Crustal Structure of Adirondacks determined from broadband teleseismic waveform modelling, *J. Geophys. Res.*, **92**, 6391-6401.

OWENS, T.J. and R.S. CROSSON (1988): Shallow structure effect on brodband teleseismic *P* waveforms, *Bull. Seismol. Soc. Amer.*, **78**, 96-108.

OWENS, T.J., G. ZANDT and S.R. TAYLOR (1984): Seismic evidence for ancient rift beneath the Cumberland Plateau, Tennessee: a detailed analysis of broadband teleseismic *P* waveforms, *J. Geophys. Res.* **89**, 7783-7795.

OWENS, T.J., R.S. CROSSON and M.A. HENDRICKSON (1988): Constraints on the subduction geometry beneath Western Washington from broadband teleseismic waveform modelling, *Bull. Seismol. Soc. Amer.*, **78**, 1319-1334.

PAROTTO M. and A. PRATURLON (1975): Geological summary of the Central Apennines, «Structural Model of Italy», CNR, *Quad. Ric. Sc.*, **90**, 275-311.

SALVINI, F. and M. TOZZI (1986): Evoluzione tettonica recente del margine tirrenico dell'Appennino centrale in base ai dati strutturali: implicazioni per l'evoluzione del Mare Tirreno, *Mem. Soc. Geol. It.*, **36**, 233-241.

SELVAGGI, G. and A. AMATO (1992): Intermediate-depth earthquakes in Northern Apennines (Italy): Evidence for a still active subduction?, *Geophys. Res. Lett.*, **19**, 2127-2130.

(received December 29, 1993;
accepted August 26, 1994)